nature climate change

LETTERS

PUBLISHED ONLINE: 24 FEBRUARY 2013 | DOI: 10.1038/NCLIMATE1827

Reductions in labour capacity from heat stress under climate warming

John P. Dunne*, Ronald J. Stouffer and Jasmin G. John

A fundamental aspect of greenhouse-gas-induced warming is a global-scale increase in absolute humidity[1,2]. Under continued warming, this response has been shown to pose increasingly severe limitations on human activity in tropical and mid-latitudes during peak months of heat stress[3]. One heat-stress metric with broad occupational health applications[4–6] is wet-bulb globe temperature. We combine wet-bulb globe temperatures from global climate historical reanalysis[7] and Earth System Model (ESM2M) projections[8–10] with industrial[4] and military[5] guidelines for an acclimated individual's occupational capacity to safely perform sustained labour under environmental heat stress (labour capacity)—here defined as a global population-weighted metric temporally fixed at the 2010 distribution. We estimate that environmental heat stress has reduced labour capacity to 90% in peak months over the past few decades. ESM2M projects labour capacity reduction to 80% in peak months by 2050. Under the highest scenario considered (Representative Concentration Pathway 8.5), ESM2M projects labour capacity reduction to less than 40% by 2200 in peak months, with most tropical and mid-latitudes experiencing extreme climatological heat stress. Uncertainties and caveats associated with these projections include climate sensitivity, climate warming patterns, CO_2 emissions, future population distributions, and technological and societal change.

Experientially, the approximate constancy of relative humidity under climate warming[1] is unlike the diurnal cycle where peak temperatures lower relative humidity, but more like the eastern US seasonal cycle where seasonal peak temperatures have high absolute humidity. Although much climate change research has focused on surface air temperature[11], assessments of moist temperature change have been limited. Much existing work has focused on extremes associated with heat waves[12], but its applicability in the climate change context is challenged as heat wave severity is often attributable to lack of local adaptation rather than adapted tolerance. Globally, humans are adapted to temperatures exceeding both human skin temperature (35 °C), and even core temperature (37 °C), through evaporative cooling, making dry air temperature an unreliable indicator of heat stress. However, although humans can endure high activity levels at high temperature for hour-scale periods, adverse reactions in even healthy and adapted individuals are well-documented under longer term exposure[6].

Climate model experiments with idealized 1% yr^{-1} CO_2 increase[3] have demonstrated the relative heat stress vulnerability of southeast Asia, southeastern US and northern Australia to climate warming using the Steadman heat index[13]. Subsequent studies have projected regional to global heat index threshold exceedances[14] and used various physiologically based heat stress indices[15,16] including specifically discussing impacts in the workplace[17]. Among the various indices available[18], the wet-bulb globe temperature index (WBGT = 0.7× wet-bulb temperature[19] (×WBT) + 0.3 × globe temperature) has the advantage of being well validated for environmental heat stress occupational thresholds for industrial[4,6] and United States military[5] labour standards (see Supplementary Information for further discussion of these indexes).

In the present study, we explore climate-change consequences under increased WBGT. Ignoring direct radiative effects, we approximate the globe temperature as dry air temperature (T_{ref}) assuming full shade and night adaptation and optimization of structures, clothing, activity scheduling and so on for thermal modulation of diurnal variability to avoid peak temperatures and direct sunlight. We further ignore weather-scale extremes and wind effects. We analyse National Center for Environmental Prediction (NCEP)/National Center for Atmospheric Research reanalysis for 1948–2011[7] and National Oceanic and Atmospheric Administration Geophysical Fluid Dynamics Laboratory (GFDL) Earth System Model[8] (ESM2M) simulations of historical and Representative Concentration Pathways (RCP) scenarios for 1861–2200[9,10] that contributed to the fifth Coupled Model Intercomparison Project[20]. We focus on two RCP scenarios: the highest scenario considered in which CO_2 concentrations continue to increase through 2200 (RCP 8.5), and an active mitigation scenario in which CO_2 concentrations begin to stabilize after 2060 to 543 ppm by 2115 (RCP 4.5).

ESM2M has its physical origin in a previous GFDL climate model[21] and has been shown to have similarly medium transient and equilibrium climate sensitivities of 1.5 °C and 3.2 °C, respectively[22], compared to the assessed likely range among climate models of 1–3 °C and 2–4.5 °C, respectively[23]. It captures regional surface climate patterns[24], modes of interannual variability[25] and historical climate change[26]. Recognizing ESM2M limitations in representing mean climate, we bias-corrected ESM2M decadal-average monthly maximum to the reanalysis. Recognizing ESM2M limitations in representing interannual variability, we also bias-corrected the decadal maximum monthly mean WBGT to the reanalysis, averaging 1.0 °C higher than the decadal-average monthly maximum (see Supplementary Information for details). Note that because daily maximum WBGT is typically 2 °C higher than monthly maximum WBGT, a monthly WBGT of 33 °C probably includes days averaging 35 °C.

The top panels of Fig. 1 represent the maximum monthly WBGT in the reanalysis for the 1970s (1971–1980; Fig. 1a) and the relatively modest increase from the 1970s into the past decade (2001–2010; Fig. 1b). Effectively, the shaded areas correspond to places where month-long environmental heat stress already results

Geophysical Fluid Dynamics Laboratory/National Oceanic and Atmospheric Administration, Princeton, New Jersey 08540-6649, USA.
*e-mail: john.dunne@noaa.gov.

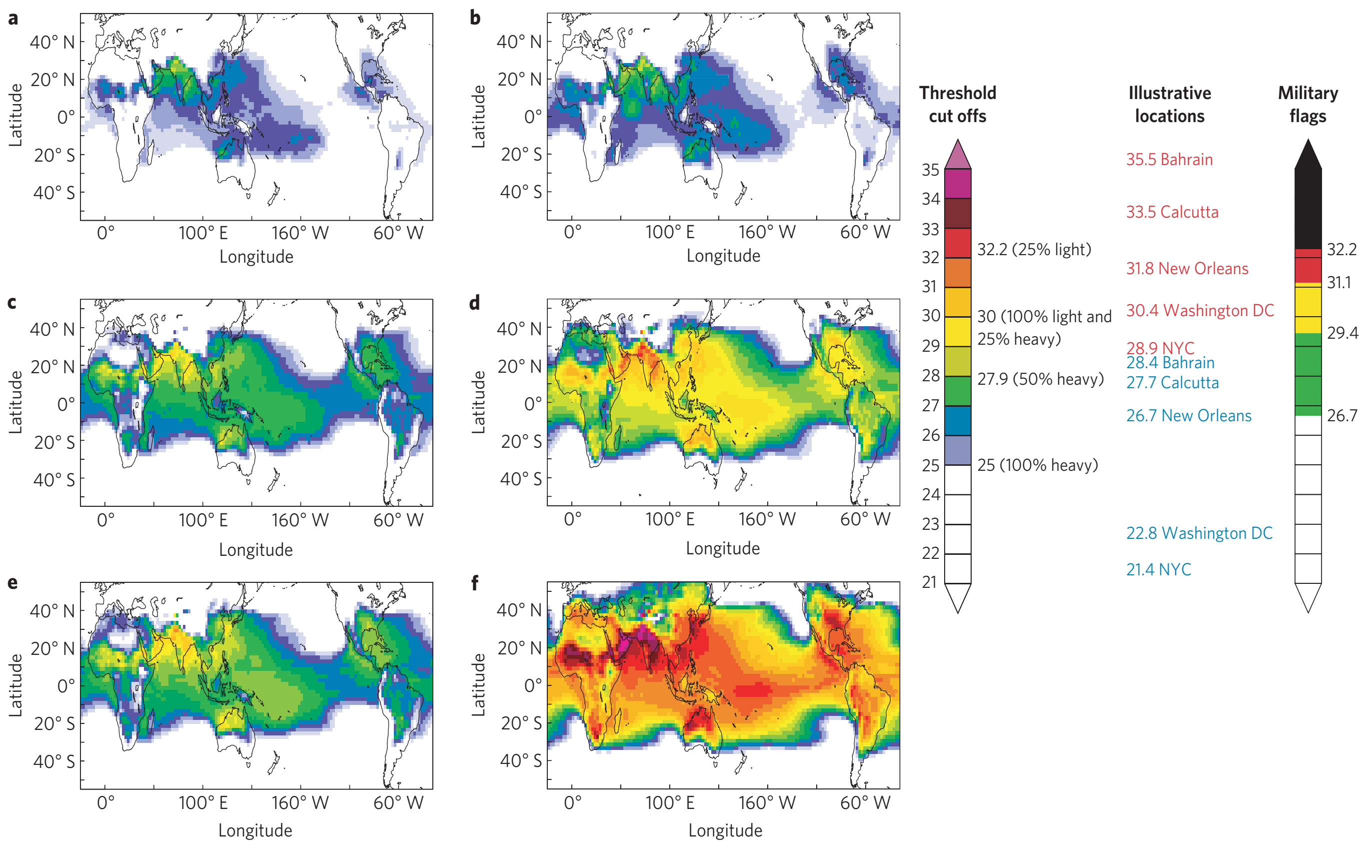

Figure 1 | Ten-year maximum monthly mean WBGT from WBT and 2 m reference temperature (T_{ref}) as a proxy for globe temperature (WBGT = 0.7 x WBT + 0.3 x T_{ref}; °C) from ESM2M T_{ref}, 2 m reference relative humidity, and surface pressure after mean and variance bias correction to reanalysis. (See Methods and Supplementary Information for details.) **a–f**, Recent past (1971–1980; **a**), most recent decade (2001–2010; **b**), projected 2091–2100 under RCP 4.5 (**c**), projected 2091–2100 under RCP 8.5 (**d**), projected 2191–2200 under RCP 4.5 (**e**), projected 2191–2200 under RCP 8.5 (**f**). **g**, Three alternative temperature scales that correspond to temperature are shown: threshold cut-off values for labour ranging from 100% (continuous) heavy labour (25 °C) to the 25% limit for heavy (30 °C), and light labour (32.2 °C); illustrative locations where present-day (blue) and RCP 8.5 2200 (red) WBGT were attained over a decade at various locations in the reanalysis-corrected model; and military flags signalling hazardous heat-stress warnings[5] named black, red, yellow, green and white, where thresholds are set between flag designations. Note that the locations are given for general illustrative purposes only, and the numbers are not suitable for local interpretation. Also shown is the global change in spatially and temporally averaged T_{ref} relative to a 1861–1960 reference period. All estimates are bias-corrected to climatological maximum monthly WBGT estimates for 1948–2011 from NCEP (ref. 7), with the decadal maximum month from NCEP added as an anomaly to the decadal climatology.

in reduction of the labour capacity of an individual as set by the environment beyond typical adaptations. The middle set of panels of Fig. 1 show projections for the end of the twenty-first century under both active mitigation of CO_2 emissions (RCP 4.5; Fig. 1c) where global surface temperature rises 1.6 °C from a 1861–1960 reference period, and the highest scenario considered (RCP 8.5; Fig. 1d) with double the warming (global $\Delta T_{ref} = 3.4$ °C). Thus, whereas ESM2M under RCP 4.5 stays near the common policy target of 2 °C (ref. 27) at 2100, ESM2M under RCP 8.5 does not.

Qualitatively similar to previous work[3], climatological heat stress changes highlight the relative vulnerability of southeast Asia, southeastern US and northern Australia. By 2100 under active mitigation (Fig. 1c), the high stress of present-day India (green Fig. 1b) expands over much of Eurasia and the greater Caribbean region (green in Fig. 1c). Under the highest scenario considered, by 2100 (Fig. 1d) much of the tropics and mid-latitudes experience months of extreme heat stress, such that heat stress in Washington DC becomes higher than present-day New Orleans, New Orleans exceeds present-day Bahrain, and Bahrain reaches a WBGT of 31.5 °C. Note that we reference only the model location of these cities for illustrative purposes and that WBGT may be further amplified owing to urban-heat-island effects, a potentially important effect both under present-day and future conditions[28,29] that is not explicitly addressed here.

Continuing these projection scenarios forward another century illustrates an even starker contrast. Extension of the RCP 4.5 scenario to 2200 yields moderate continued warming (Fig. 1e; global $\Delta T_{ref} = 2.3$ °C). Extension of the highest emission scenario (RCP 8.5) to 2200 (Fig. 1f; global $\Delta T_{ref} = 6.2$ °C), in contrast, leaves much of the tropics and mid-latitudes experiencing extreme climatological heat stress, with Washington, DC and New York well exceeding heat stress levels of present-day Bahrain.

To quantify the projected implications for human activity, we used industrial[4] and military[5] guidelines on threshold limit values for safety in occupational labour. This metric is a guideline for moderating labour during a typical 8-h work day to reduce the threat of hyperthermia and its effects. For continuous representation of these thresholds, we derived an algorithm including percentage limits for heavy (350–500 kcal h^{-1}), moderate (200–350 kcal h^{-1}) and light (<200 kcal h^{-1}) labour, noting that moderate and light labour can be renormalized to heavy labour for a single fit (Fig. 2, inset). Note that light labour would be equivalent to walking, and even heavy labour (for example, occupational lifting, carrying, digging and so on) is defined as activity far less exertive than marathon running (~1,000 kcal h^{-1}). Although not

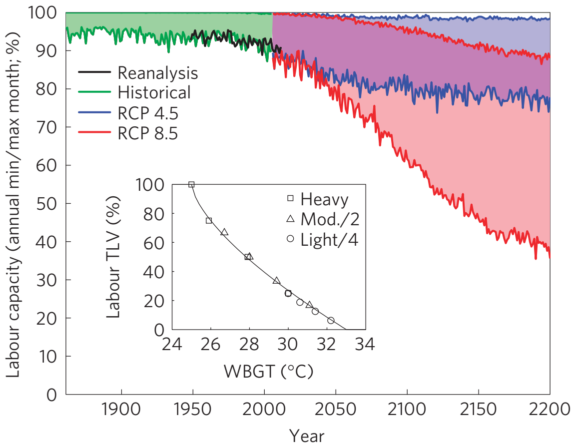

Figure 2 | Population-weighted individual labour capacity (%) during annual mimimum (upper lines) and maximum (lower lines) heat stress months. Shown are the historical period (NCEP reanalysis—black, maximum alone; ESM2M historical—green), RCP 4.5 (blue) and RCP 8.5 (red) derived as in the inset[4,6] (symbols for heavy, moderate and light labour threshold limit values) through a continuous representation (labour capacity $= 100 - 25 \times \max(0, \text{WBGT} - 25)^{2/3}$ with an upper bound of 100; black line in inset); WBGT was derived as in Fig. 1. The 2010 population distribution was taken from Columbia University's Center for International Earth Science Information Network Gridded Population of the World (http://sedac.ciesin.columbia.edu/gpw).

a direct physiological limit, this metric represents safety standards for a healthy, acclimated individual's capacity to safely perform heavy labour under environmental heat stress (labour capacity). This allows us to quantify the global significance of heat stress on lost labour capacity weighted by the 2010 geographical population distribution (Fig. 2). Reduction of labour capacity during the reanalysis period varies between 0% (boreal winter) and 4–10% (boreal summer) with an overall increase in the maximum from a range of 4–8% from 1948–1987 to 6–10% after 1990 with the peak during the 1998 La Niña. As in Fig. 1, the climatological maximum and its variability in ESM2M have been bias-corrected to the reanalysis. Under historical forcing, ESM2M (green) compares well to the reanalysis after bias-correction. Under both RCP 4.5 (blue) and RCP 8.5 (red) by 2050, global lost labour capacity increases in the maximum months to approximately double that in the historical period. Beyond 2050, active mitigation in RCP 4.5 results in reduction of labour capacity to 75% in peak months. Thus, even active mitigation to limit global warming to a 2 °C change from pre-industrial conditions[27] results in roughly a doubling of the reduction in lost labour capacity in this model. (Note: ESM2M's moderate climate sensitivity among climate models allows it to limit warming to 2 °C even under RCP 4.5. As shown in the Supplementary Information, CMIP5 models commonly have higher sensitivities than ESM2M such that only under the lower RCP 2.6 scenario do these models generally limit warming to 2 °C.) Alternatively, the highest scenario considered (RCP 8.5; red) reduces labour capacity to 63% by 2100 in the hottest months (lower red line in Fig. 2). By 2200, this reduces to 39% in the hottest months (lower red line in Fig. 2). In addition, maximum monthly labour capacity in this scenario (upper red line in Fig. 2) ceases to be greater than 88% at any time of year as Southern Hemisphere population is increasingly impacted. In this scenario, 12% of the present population distribution meets or exceeds the threshold limit for industrial 25% light labour and military black flag (32.2 °C) by 2200.

Given the gravity of potential human impacts discussed here, it is important to characterize the uncertainties. One uncertainty is in the emission scenarios themselves. By 2200, the RCP 8.5 scenario assumes 4.8 Eg C is emitted after 2005. Latest estimates[30] project about 1–2 Eg C in reserves and 8–14 Eg C in further resources of detected quantities that cannot profitably recovered at present, but might be recoverable in the future assuming technological advances and increasing future resource prices. Others argue on the basis of past exploited reserves that these projections are unrealistic, and that realized past and future coal extraction will be far lower[31,32]. Although assuming similar technological and economic constraints as RCP 8.5, RCP 4.5 alternatively assumes that the global community actively commits to effective emissions mitigation. For any future scenario, projected population growth and distribution and economic, technological and societal changes are highly uncertain (see Supplementary Information for sensitivity study). Another uncertainty is the relationship of CO_2 emissions to atmospheric CO_2 concentrations based on land and ocean uptake[33]. Yet other uncertainties include the transient and equilibrium climate sensitivity[23] (see Supplementary Information for select comparison with other models), representation of interannual variability in maximum WBGT and its potential to change scope, and the relation of monthly average conditions to the diurnal cycle, weather and spatial patterns. Although model uncertainty in regional patterns give ranges roughly equivalent to the magnitude of warming[33], recent work has demonstrated that the WBGT metric is particularly insensitive to this variation owing to the compensation between temperature and relative humidity changes[34]. In focusing on the capacity of healthy, acclimated individuals, this study also severely underestimates heat stress implications for less-optimally acclimated individuals. Importantly, by focusing on heat stress alone, the present study also ignores potential enhancements to global agricultural labour productivity under climate warming due to CO_2 fertilization and longer growing seasons, and labour productivity increases associated with reduction in adverse conditions of extreme cold, snow and frozen soil—all factors worthy of further investigation.

Overall, we show that consideration of the moist thermal response under climate warming poses increasingly severe environmental limitations on individual labour capacity as set by occupational standards in the coming decades, specifically in lost labour capacity in the peak months of heat stress, even if the global community commits to active mitigation of CO_2 emissions (RCP 4.5). We demonstrate that projections out to 2200 under the highest CO_2 scenario considered (RCP 8.5) expose most of the present population distribution to extreme heat stress in peak months, prohibit any safe labour in large areas, and expose mid-latitude regions such as the US east of the Rockies to environmental heat stress experienced only by the most extremely hot regions of the present day.

Methods

We calculate the WBT using the Davies-Jones method[9] for temperatures between 0 and 100 °C:

$$\begin{aligned} e_{sat} = {} & \exp(-2{,}991.2729/T_{ref}^2 - 6{,}017.0128/T_{ref} \\ & + 18.87643854 - 0.028354721 \times T_{ref} \\ & + 1.7838301 \times 10^{-5} \times T_{ref}^2 - 8.4150417 \times 10^{-10} \times T_{ref}^3 \\ & + 4.4412543 \times 10^{-13} \times T_{ref}^4 + 2.858487 \times \ln(T_{ref}))/100 \end{aligned} \quad (1)$$

$$w_{sat} = 621.97 \times e_{sat}/(p - e_{sat}) \quad (2)$$

$$w = \text{rh}_{ref}/100 \times w_{sat} \quad (3)$$

$$T_L = 1/(1/(T_{ref} - 55) - \ln(\text{rh}_{ref}/100)/2{,}840) + 55 \quad (4)$$

$$\begin{aligned} \theta_E = {} & T_{ref} \times (1{,}000/p) \wedge (0.2854 \times (1 - 0.28 \times 10^{-3} \times w)) \\ & \times \exp((3.376/T_L - 0.00254) \times w \times (1 + 0.81 \times 10^{-3} \times w)) \end{aligned} \quad (5)$$

$$\mathrm{WBT} = 45.114 - 51.489 \times (\theta_E/273.15)^{-3.504} \quad (6)$$

T_{ref} is the absolute temperature (K) at a reference level of 2 m, rh_{ref} is the relative humidity at a reference level of 2 m (allowed to range between 0.01% and 100%), p is the surface pressure (mbar), e_{sat} is the saturation vapour pressure (mbar) obtained from equation 9 of ref. 35 (derived from ref. 36), w_{sat} is the saturation mixing ratio (g kg^{-1}), w is the mixing ratio (g kg^{-1}), T_L is the lifting condensation temperature (K; temperature at which relative humidity would reach 100% on adiabatic lifting) and θ_E is the equivalent potential temperature (K; temperature a parcel of air would reach if it were continued to be adiabatically lifted to condense all water, and then lowered dry adiabatically to 1,000 mbar) obtained from Bolton (1980) equation 43. Note that the WBT also has an upper bound of dry-bulb temperature in degrees Celsius (that is, $\mathrm{WBT} \leqq T_{ref} - 273.15$). As a check value, input values of $T_{ref} = 303.15$ K, $rh_{ref} = 50\%$ and $p = 1{,}000$ mbar give WBT = 22.25 °C.

To correct for ESM2M biases in the climatological maximum, we calculated a monthly climatology for both ESM2M and NCEP and then took the difference between the maximum for each climatology to apply as an anomaly for a mean-corrected WBGT ($\mathrm{WBGT^{MC}}$; Supplementary Fig. S3a). The correction for ESM2M's relative excess in decadal-scale variability and resulting extremes (Supplementary Fig. S3b) was more involved. Over the NCEP reanalysis period of 1948–2011, there is considerable inter-annual variability as well as a long-term trend. To isolate biases in variability on the decadal scale, we binned the NCEP and ESM2M data into six decades (that is 1951–1960 to 2001–2010). For each decade, we calculated a monthly climatology. We then calculated the difference between the decadal maximum and the climatological maximum for each decade. This gave six estimates of historical decadal-scale departure beyond the decadal climatological maximum month, which we then averaged for a single decadal maximum anomaly estimate for both NCEP ($\mathrm{WBGT^{NCEP\_DMA}}$) and ESM2M ($\mathrm{WBGT^{DMA}}$). To normalize the model variability to this scaling, we first calculated the annual maximum WBGT ($\mathrm{WBGT^{AM}}$), and then the decadal mean maximum ($\mathrm{WBGT^{DM}}$) as the 10-year box-car smoothed values of $\mathrm{WBGT^{AM}}$ by filling in the beginning and ending decades with median values for those decades. We then calculate the variance corrected WBGT ($\mathrm{WBGT^{VC}}$) as:

$$\mathrm{WBGT^{VC}} = \mathrm{WBGT^{MC}} - (\mathrm{WBGT^{AM}} - \mathrm{WBGT^{DM}}) \times (1 - \mathrm{WBGT^{NCEP\_DMA}}/\mathrm{WBGT^{DMA}})$$

Note that this is applied only when $\mathrm{WBGT^{NCEP\_DMA}}/\mathrm{WBGT^{DMA}}$ is less than one to reduce ESM2M variability only to levels of NCEP and avoid adding variability where NCEP gave more variability than ESM2M.

We combine light, moderate and heavy labour into a single metric through the observation that the definition of light labour corresponds to roughly 50% of moderate labour, and that moderate labour corresponds to roughly 50% of heavy labour. The three metrics can then be plotted (Fig. 2, inset) on the same WBGT axis along a continuum from 25 °C(threshold limit value for 100% 'heavy' labour) to 32.2 °C (threshold limit value for 25% 'light' labour). Our best fit to these data was achieved through:

$$\mathrm{labour\_capacity} = 100 - 25 \times \max(0, \mathrm{WBGT} - 25)^{2/3}$$

This function extrapolates to a limit of 0% 'light' labour at 33 °C and an upper bound at 100%.

Received 8 August 2012; accepted 15 January 2013; published online 24 February 2013

References

1. Manabe, S. & Wetherald, R. T. The effects of doubling CO_2 concentration on the climate of a general circulation model. *J. Atmos. Sci.* **32,** 3–15 (1975).
2. Manabe, S. & Stouffer, R. J. A CO_2-climate sensitivity study with a mathematical model of the global climate. *Nature* **282,** 491–493 (1979).
3. Delworth, T. L., Mahlman, J. D. & Knutson, T. R. Changes in heat index associated with CO_2-induced global warming. *Climatic Change* **43,** 369–386 (1999).
4. American Conference of Governmental Industrial Hygienists *Threshold Limit Values for Chemical Substances and Physical Agents. Biological Exposure Indices* (ACGIH, 1996).
5. *Heat Stress Control and Heat Casualty Management* Technical Bulletin Medical 507/Air Force Pamphlet 48-152 (US Army, 2003).
6. Parsons, K. Heat stress standard ISO 7243 and its global application. *Ind. Health* **44,** 368–379 (2006).
7. Kalnay, E. *et al.* The NCEP/NCAR 40-Year Reanalysis Project. *BAMS* **77,** 437–470 (1996).
8. Dunne, J. P. *et al.* GFDL's ESM2 global coupled climate-carbon Earth System Models Part I: Physical formulation and baseline simulation characteristics. *J. Clim.* **25,** 6646–6665 (2012).
9. Moss, R. H. *et al.* The next generation of scenarios for climate change research and assessment. *Nature* **463,** 747–756 (2010).
10. Meinshausen, M. *et al.* The RCP greenhouse gas concentrations and their extensions from 1765 to 2300. *Climatic Change* **109,** 213–241 (2011).
11. Cubasch, U. *et al.* in *IPCC Climate Change 2001: The Scientific Basis* (eds Houghton, J. T. *et al.*) 525–582 (Cambridge Univ. Press, 2001).
12. Confalonieri, U. *et al.* in *IPCC Climate Change 2007: Impacts, Adaptation and Vulnerability* (eds Parry, M. L. *et al.*) 391–431 (Cambridge Univ. Press, 2007).
13. Steadman, R. G. The assessment of sultriness. Part I: A temperature–humidity index based on human physiology and clothing science. *J. Appl. Meteorol.* **18,** 861–873 (1979).
14. Willett, K. M. & Sherwood, S. C. Exceedance of heat index thresholds for 15 regions under a warming climate using the wet-bulb globe temperature. *Int. J. Climatol.* **32,** 161–177 (2012).
15. Jendritzky, G. & Tinz, B. The thermal environment of the human being on the global scale. *Glob. Health Action* **2** (Special volume), 10–21 (2009).
16. Sherwood, S. C. & Huber, M. An adaptability limit to climate change due to heat stress. *Proc. Natl Acad. Sci. USA* **107,** 9552–9555 (2010).
17. Kjellstrom, T., Holmer, I. & Lemke, B. Workplace heat stress, health and productivity—an increasing challenge for low and middle-income countries during climate change. *Glob. Health Action* **2** (Special volume), 46–51 (2009).
18. Epstein, Y. & Moran, D. S. Thermal comfort and the heat stress indices. *Ind. Health* **44,** 388–398 (2006).
19. Davies-Jones, R. An efficient and accurate method for computing the wet-bulb temperature along pseudoadiabats. *Mon. Weath. Rev.* **136,** 2764–2785 (2008).
20. Taylor, K. E., Stouffer, R. J. & Meehl, G. A. An overview of CMIP5 and the experiment design. *BAMS* **93,** 485–498 (2012).
21. Delworth, T. L. *et al.* GFDL's CM2 global coupled climate models. Part I: Formulation and simulation characteristics. *J. Clim.* **19,** 643–674 (2006).
22. Winton, M. *et al.* Influence of ocean and atmosphere components on simulated climate sensitivities. *J. Clim.* **26,** 231–245 (2013).
23. Meehl, G. A. *et al.* in *IPCC Climate Change 2007: The Physical Science Basis* (eds S., Solomon *et al.*) 747–845 (Cambridge Univ. Press, 2007).
24. Reichler, T. & Kim, J. How well do coupled models simulate today's climate? *BAMS* **89,** 303–311 (2008).
25. Guilyardi, E. *et al.* Understanding El Niño in ocean–atmosphere general circulation models. *BAMS* **90,** 325–340 (2009).
26. Hegerl, G. C. *et al.* in *IPCC Climate Change 2007: The Physical Science Basis* (eds Solomon, S. *et al.*) 663–745 (Cambridge Univ. Press, 2007).
27. Meinshausen, M. *et al.* Greenhouse-gas emission targets for limiting global warming to 2 °C. *Nature* **458,** 1158–1162 (2009).
28. McCarthy, M. P., Best, M. J. & Betts, R. A. Climate change in cities due to global warming and urban effects. *Geophys. Res. Lett.* **37,** L09705 (2010).
29. Fischer, E. M., Oleson, K. W. & Lawrence, D. M. Contrasting urban and rural heat stress responses to climate change. *Geophys. Res. Lett.* **39,** L03705 (2012).
30. Rogner, H-H. *et al. Global Energy Assessment—Toward a Sustainable Future* 425–512 (Cambridge Univ. Press and IIASA, 2012).
31. Schindler, J. & Wittel, Z. *Crude Oil: The Supply Outlook Report to the Energy Watch Group* EWG Series No 3/2007 (Energy Watch Group, 2007).
32. Rutledge, D. Estimating long-term world coal production with logit and probit transforms. *Int. J. Coal Geol.* **85,** 23–33 (2011).
33. Christensen, J. H. *et al.* in *IPCC Climate Change 2001: The Scientific Basis* (eds Houghton, J. T. *et al.*) 847–865 (Cambridge Univ. Press, 2001).
34. Fischer, E. M. & Knutti, R. Robust projections of combined humidity and temperature extremes. *Nature Clim. Change* **3,** 126–130 (2013).
35. Bolton, D. The computation of equivalent potential temperature. *Mon. Weath. Rev.* **108,** 1046–1053 (1980).
36. Wexler, A. Vapor pressure formulation for water in range 0 to 100C. A revision. *J. Res. Nat. Bur. Stand.* **80A,** 775–785 (1976).

Acknowledgements

The scientific results and conclusions, as well as any views or opinions expressed herein, are those of the authors and do not necessarily reflect the views of NOAA or the US Department of Commerce. The authors thank I. Held, T. Delworth, T. Knutson and V. Ramaswamy for constructive criticisms to improve the manuscript.

Author contributions

J.P.D. designed the study, conducted the analysis and wrote the manuscript. J.G.J. performed experiments and gave technical advice. R.J.S. provided technical and conceptual advice.

Additional information

Supplementary information is available in the online version of the paper. Reprints and permissions information is available online at www.nature.com/reprints. Correspondence and requests for materials should be addressed to J.P.D.

Competing financial interests

The authors declare no competing financial interests.